Appendix M1, M2. Supplementary Methods

"Sudden collapse of a mesopredator reveals its complementary role in mediating rocky reef regime shifts"

Proceedings of the Royal Society B – DOI: 10.1098/rspb.2018-0553

Jenn M. Burt[1,2], Tim M. Tinker[3], Daniel K. Okamoto[1,4], Kyle W. Demes[1,2,5], Keith Holmes[2], Anne K. Salomon[1,2]

1 - School of Resource and Environmental Management, Simon Fraser University, BC, Canada
2 - Hakai Institute, BC, Canada
3 - Department of Ecology and Evolutionary Biology, University of California Santa Cruz, CA, USA
4 - Department of Biological Sciences, Florida State University, Tallahassee, Florida, USA
5 - Department of Zoology, The University of British Columbia, BC, Canada

Appendix M1. Methods and the associated outputs for the analysis of size class transition probabilities using the Zhang et al. 2008 growth model.

To model transitions between urchin size classes we required estimates of size-specific growth rates, which we obtained from a recently published red urchin growth model from British Columbia (Zhang et al. 2008). In summary, we converted the growth function into stage-specific transition probabilities using a simulation model that tracked the growth of individual urchins drawn randomly from our empirically derived size distribution (combined for all sites, all years), calculated annual growth according to the published model (including stochasticity), and then computed transition probabilities as the proportion of individuals from size class *i* that transitioned to size class *i* +1 after one year. See equations and graphs below.

Zhang et al. (2008) use a Tanaka growth function within a Bayesian framework to model the growth of red sea urchins *Mesocentrotus franciscanus* (*D*) based on tag-recapture data and abundance surveys conducted in four locations on the coast of British Columbia:

$$D_{t+1} = \frac{1}{\sqrt{f}} \log\left[\left(2f\left(\frac{E}{4f} - \frac{a}{E} + 1\right) + 2\sqrt{f^2\left(\frac{E}{4f} - \frac{a}{E} + 1\right) + f * a}\right)\right] + d + \varepsilon \quad (1)$$

$$E = \exp\left(\sqrt{f}\left(D_t - d\right)\right) \quad (2)$$

where ε is a normal variate ε ~ N(0, σ2), and with other area-specific parameters defined as follows (we chose the Price Island area closest to our survey region):

Parameter	Area where data derived	Mean parameter estimate from Zhang et al. 2008
a	Price Island	0.00539
d	Price Island	118.2
f	Price Island	0.00342
σ	Price Island	1.21

We used above equations and parameter values to simulate one year of growth for 5000 individual urchins (Figure M1.1), where the initial size of urchins were drawn randomly from our empirically-derived size distribution (we combined data from all sites, all years).

We then used these simulated growth trajectories to calculate stage-specific "growth transition probabilities" (Gi). Specifically, we computed the proportion of individuals that began the year in the "small" size class (1-3 cm) and transitioned to the "medium" size class (4-7 cm) by the end of the year (G1), and the proportion of individuals that began the year in the "medium" size class and transitioned to the "large" size class (≥ 8 cm) by the end of the year (G2). To quantify uncertainty, we bootstrapped the above analyses 1000 times and plotted the distribution of estimated growth transition values (Figure M1.2). We used the median values of growth transitions (G1=0.52 and G2=0.09) to parameterize our urchin population model.

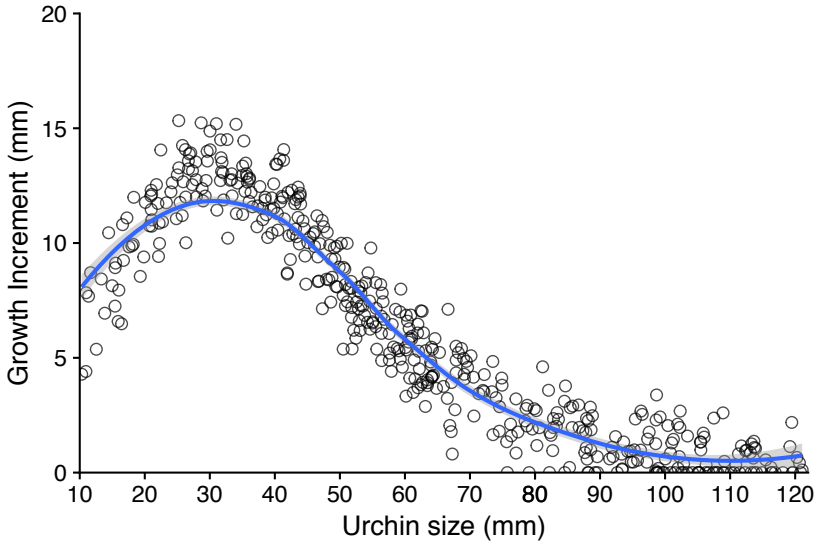

Figure M1.1 Simulated growth increment over one year for all individual urchins measured over the course of our four years of dive surveys. The blue line is a fitted smoothing spline.

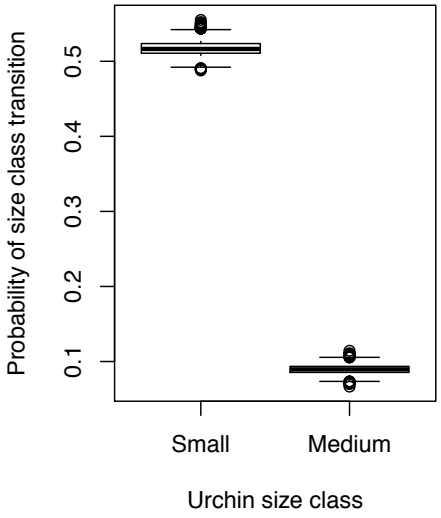

Figure M1.2 Estimated growth transition probabilities are shown as the proportion of urchins that transition from the small to medium size class (left) and medium to large size class (right). Box plots show the median value with the interquartile range, with whiskers showing the distance to the furthest values.

Appendix M2. Methods for generating, processing, and classifying aerial kelp canopy imagery.

Aerial imagery prior to sea otter arrival:

We opportunistically obtained aerial imagery for two years (2006 and 2012) prior to the arrival of sea otters in the northwest Calvert Island region in 2013 captured from the British Columbia air photo archives in 2006 (www2.gov.bc.ca/gov/content/data/about-data-management/geobc) and a terrestrial lidar survey which included nearshore waters in 2012 commissioned by the Hakai Institute (details and metadata available at https://hecate.hakai.org/).

Because the 2006 and 2012 images were captured at higher tide heights compared to the 2014, 2015, 2016 images generated in our aerial surveys (where all tides < +1.0 m), we applied a correction factor to compensate for tide-related underestimates of kelp canopy extent prior to sea otter arrival. Data to calculate the correction factor was generated in 2015: We selected a 20 hectare sub-sample within the study region that contained a mix of high and low density kelp beds of variable sizes and used drones to generate aerial imagery (see methods below) captured at three tide heights: 0.25 m, 2.5 m, and 3.0 m. We performed a simple linear regression using the total area of kelp cover (m^2) observed at these three tide heights. With this relationship, we calculated the percent reduction in canopy kelp area between the imagery tide heights and a +0.25 m tide height (23% reduced at a 2.5 m tide in 2006, 16% reduced at a 1.8 m tide in 2012). We then multiplied the extent of all kelp beds from the 2006 and 2012 by the equivalent correction factors, 1.23 and 1.16, respectively.

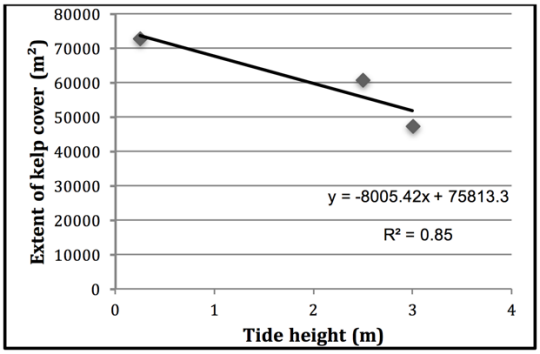

Annual aerial surveys post sea otter arrival:

Starting in 2014, we conducted annual aerial surveys of the surface canopy kelp in the northwest Calvert Island region. In 2014, 2015, and 2016, the aerial surveys were conducted in the first low tide sequence in August, which is within the seasonal time period (August – October) that corresponds to maximum canopy extent in British Columbia. All imagery capture occurred during low tide cycles at tide heights below +1.0 m and during periods where environmental conditions were favorable: calm seas (sea state less than 1.5 m swell), clear visibility (no fog or low-lying cloud), and low winds (less than 15 knots).

In 2014, we obtained kelp canopy imagery taken from a helicopter using a Canon EOS MarkII camera with a Canon EF 16-35mm f/2.8L II USM lens. The images were taken at 800 m altitude over a period of 25 minutes. We then processed the images into a mosaic using the program Autostitch v.2.2 (http://matthewalunbrown.com/autostitch/autostitch.html). After stitching was complete the mosaic was georeferenced in ARC GIS 10.0 to the 2012 reference imagery using a spline transformation.

In 2015 and 2016, we conducted aerial kelp canopy surveys using DJI Phantom 3 professional Unmanned Aerial Vehicles (UAVs or drones) equipped with a commercial grade 12 megapixel 4k f 2.8 lens RGB camera to capture imagery. We conducted a continuous series of UAV flights from a small research vessel moving in a pre-planned grid formation through the

study region and operated the UAV and camera using the *DJI Capture* software application connected to a tablet. Flights ranged from 12 – 17 minutes at a flight level of approximately 200-250 m (results in images 8-12 cm in spatial resolution), which allowed an area of 1.5 x 1.5 km to be covered in one flight. We captured adjacent images with a minimum overlap of 85% to ensure sufficient coverage and to give us the flexibility to select out images of poor quality.

Imagery processing:

We gathered and stored the UAV images with relevant field condition metadata (date, time, location, pilot, weather, tide, flight elevation, grid size, UAV application used, notes). We used Pix4D image processing software to mosaic and project the UAV images into a .tiff file format. Within Pix4D, we selected the images to produce a full image report which we checked to ensure no gaps or major errors were transferred to the final map product. Finally, we digitally stamped the fully processed image mosaic with the time, compass bearing, and GPS location and loaded it into ARC GIS 10.2 for georeferecing. For all the survey image mosaics produced, we used the 2012 orthophoto imagery at 25 cm spatial resolution as the georeference. The 2012 imagery was validated with a survey grade GPS to ensure that all images georeferenced to it achieved a sub meter accuracy.

Manual classification of kelp beds:

We loaded the time series of aerial images into ARC GIS 10.2 and manually classified the kelp extents. Classification resulted in a shapefile layer (.shp) of kelp bed polygons with a number of associated attributes: species (*M. pyrifera* or *N. luetkeana*), bed area (m^2), mapper name, mapper confidence (high, medium, low), and bed density (high or low). We applied the following decision rules during the mapping process: 1) Individual kelp beds are delineated areas of consistent kelp density: either 'high density' (> 10 plants per $10m^2$) or 'low density' (< 10 plants/fronds per $10m^2$) based on the B.C. Province's Kelp Inventory Method (Foreman 1975[1]), 2) A "kelp bed" consists of at least three adjacent plants/fronds, and 3) Individual kelp beds are considered distinct if they are separated by a gap larger than 5 m whereas kelp plants or patches within 5 m of each other are considered part of the same bed. Following initial kelp bed classification, the final classified polygon layers were quality control checked by the same individual who utilized field notes and corresponding high-resolution imagery confirm kelp beds classified with 'low confidence'.

[1] Foreman, R.E. (1975). *KIM-1: A method for inventory of floating kelps and its application to selected areas of kelp license area 12*. Final Report to Marine Research Branch, Dept. of Recreation and Conservation. Province of B.C. BERP report 75-1. 81 pp.